https://doi.org/10.5194/bg-2022-135
Preprint. Discussion started: 29 June 2022
© Author(s) 2022. CC BY 4.0 License.

Biogeosciences Discussions
Open Access
EGU

The highest methane concentrations in an Arctic river are linked to local terrestrial inputs.

Karel Castro-Morales[1*], Anna Canning[2], Sophie Arzberger[1], Will A. Overholt[1], Kirsten Küsel[1,3], Olaf Kolle[4], Mathias Göckede[4], Nikita Zimov[5], and Arne Körtzinger[2,6]

[1] Friedrich-Schiller University Jena, Institute of Biodiversity, Jena, Germany.
[2] GEOMAR Helmholtz Centre for Ocean Research Kiel, Kiel, Germany.
[3] German Centre for Integrative Biodiversity Research (iDiv) Halle-Jena-Leipzig, Germany
[4] Max Planck Institute for Biogeochemistry, Jena, Germany
[5] Pleistocene Park, Northeast Science Station, Chersky, Russia.
[6] Christian Albrecht University Kiel, Kiel, Germany

***Correspondence:** Karel Castro-Morales (karel.castro.morales@uni-jena.de)

Abstract.

Large amounts of methane (CH_4) could potentially be formed as a result of the gradual or abrupt thawing of Arctic permafrost due to global warming. Upon its release, this potent greenhouse gas can be emitted into the atmosphere, or transported laterally into aquatic ecosystems via hydrologic connectivity at surface or groundwaters. While high northern latitudes contribute up to 5 % of total global CH_4 emissions, the specific contribution of Arctic rivers and streams is largely unknown. In this study, we measured high-resolution continuous CH_4 concentrations in a ~120 km section of the Kolyma River in Northeast Siberia navigated twice between 15-17 June 2019 (late freshet). The average partial pressure of CH_4 (pCH_4) in tributaries (66.8 – 206.8 µatm) was 2-7 times higher than in the main river channel (28.3 µatm). In the main channel, CH_4 was up to 1600 % supersaturated with respect to atmospheric equilibrium. At key sites located near the riverbank and tributary confluences, pCH_4 (41±7 µatm) and emissions (0.03±0.004 mmol m^{-2} d^{-1}) were higher compared to other sites within the main channel. Warm waters (T>14.5 °C) and low specific conductivities (κ<88 µS cm^{-1}) defined these key sites. The distribution of methane in the river could also be linked statistically to T and κ of the water, as well as to the distance to the shore z, as indicators used to predict CH_4 concentrations in unsampled river areas. Similarly, the abundance of methane consuming bacteria and methane producing archaea strongly correlated mainly to T and κ, and less to the pCH_4, and were similar to those previously detected in nearby soils, suggesting the source of CH_4 to be associated with sites close to land. The average total CH_4 flux densities in the investigated Kolyma River section were 0.02±0.006 mml m^{-2} d^{-1}, equivalent to a total CH_4 flux of 12.4 mmol m^{-2}. Key sites with highest CH_4 concentrations contributed from 13 to 20 % to the total flux. Our study highlights the importance of high-resolution continuous CH_4 measurements in Arctic Rivers for identifying spatial and temporal variabilities, and offers a glimpse to the magnitude of riverine methane emissions in the Arctic and their potential relevance to regional methane budgets.

https://doi.org/10.5194/bg-2022-135
Preprint. Discussion started: 29 June 2022
© Author(s) 2022. CC BY 4.0 License.


1 Introduction

Methane (CH_4) is a powerful greenhouse gas that absorbs the Earth's infrared radiation more efficiently than CO_2, with a global warming potential 28 times that of CO_2 over a time horizon of 100 years (Saunois et al., 2020). To date, methane has accounted for 16 to 25 % of the current atmospheric warming (Etminan et al., 2016; IPCC, 2014; Rosentreter et al., 2021). Globally, aquatic ecosystems contribute about half (53 %) of the total CH_4 emissions, both from anthropogenic and natural origin (Rosentreter et al., 2021). The total bottom-up (i.e., from process-based models and inventories) updated global CH_4 emissions from rivers and streams have a mean of 30.5±17.1 Tg CH_4 yr^{-1} (Rosentreter et al., 2021), and account for ~17 % of the average inland water CH_4 fluxes (Saunois et al., 2020). Especially on regional scales, CH_4 emissions from rivers and streams have large impacts on the estimation of local atmospheric emissions (Karlsson et al., 2021). The contribution of CH_4 emissions in high northern latitudes (60 – 90° N) to total global CH_4 emissions ranges between 4 to 5 %, but there are significant uncertainties, particularly regarding the contributions from terrestrial permafrost and non-wetland inland waters, i.e., rivers, streams, and lakes (Saunois et al., 2020). The concentration of CH_4 in rivers and streams is generally above saturation with respect to the present atmospheric CH_4 concentration, emitting annually the equivalent to ~15 % of the total emissions from wetlands or 40 % of the annual CH_4 emissions from lakes (Stanley et al., 2016).

The Arctic Ocean is one of the most river-influenced and land-locked of all the world oceans (Charkin et al., 2017; Shakirov et al., 2020), receiving annually about 10 % of the global runoff (Lammers et al., 2001), through the input from the main six Arctic rivers: Yenisey, Lena, Ob, Mackenzie, Yukon, and Kolyma. These rivers connect the ocean with the land, by mediating the transport of CH_4 stored in terrestrial surface waters or groundwaters, or through soil-water interactions in thawed water tracks (Connolly et al., 2020; Dabrowski et al., 2020; Harms et al., 2020; Saunois et al., 2020). Thus, the riverine transport of soil-derived CH_4 from permafrost may influence the CH_4 concentrations in the Arctic shelf system.

The atmospheric emissions of CH_4 from Arctic inland freshwaters and permafrost have the potential to increase with climate change (Dean et al., 2018). As permafrost thaws, more soil organic carbon is available for the anaerobic degradation of organic matter under warmer conditions, resulting in additional CH_4 formation of which will add to the positive feedback to climate change (Schuur et al., 2015). Trapped or newly formed CH_4 can be emitted directly to the atmosphere after the abrupt or gradual permafrost thaw (Olefeldt et al., 2013; Saunois et al., 2020; Turetsky et al., 2020), or be laterally transported into neighboring inland waters via

https://doi.org/10.5194/bg-2022-135
Preprint. Discussion started: 29 June 2022
© Author(s) 2022. CC BY 4.0 License.


surface hydraulic connectivity or underground drainage (e.g., Dabrowski et al., 2020). Current and projected changes in the Arctic land surface hydrology, vegetation, landscape, and temperature due to permafrost thaw, will modulate CH_4 concentrations in Arctic fluvial ecosystems (Harms et al., 2020; Olid et al., 2021).

The magnitude of the fluvial CH_4 emissions is subject to strong local environmental controls, because CH_4 has low solubility in water (Campeau and del Giorgio, 2014; Stanley et al., 2016). At the same time, the abundance and phylogenetic identity of microorganisms in the river water that can be associated to the formation or consumption of CH_4, can serve as indicators of the source and fate of CH_4 transported from land. Aquatic CH_4 is subject to microbial oxidation and photochemical decomposition (Dean et al., 2018; Stanley et al., 2016). Little is known about the magnitude of CH_4 concentrations and emissions from flowing Arctic inland waters, as well as how they vary over time and space. Point CH_4 measurements in some Arctic rivers and streams have demonstrated supersaturation relative to the atmosphere (e.g., Kling et al., 1992; Mann et al., 2022; Striegl et al., 2012; Vorobyev et al., 2021; Zolkos et al., 2019). However, highly resolved aquatic CH_4 measurements are lacking in large portions of Arctic rivers and streams, and these are needed to better quantify the atmospheric gas fluxes and understand the temporal variations and the environmental indicators. High-resolution measurements of the partial pressure of methane (pCH_4) were measured in a site in Ambolikha River, a tributary of Kolyma River in northeast Siberia, evidencing aquatic CH_4 supersaturations up of the order of 200 times higher than values at equilibrium with the atmosphere. These measurements allowed identifying temporal variations mostly driven by hydrological changes and air-water exchange, with a consistent decrease of pCH_4 by 78 % from the measured concentrations during late freshet to summer (Castro-Morales et al., 2022).

Here, we present the first high spatial resolution measurements of pCH_4, and other complementary water properties, in a large section of the Kolyma River during the late freshet (June) in 2019. Additionally, we followed the riverine microbial community structure using a 16S-amplicon approach along the same 120 km long transect, to provide a potential record of water input sources. The objectives of this study are: 1) to analyze potential environmental indicators that can be statistically associated with the spatial variations of the pCH_4 along the sampled river section, 2) to estimate the flux of CH_4 across the atmosphere-river interface, and 3) to investigate a potential link between overall microbial community structure and more specifically the distributions of methane oxidizers and methane producer with the measured pCH_4 during the sampling period.

https://doi.org/10.5194/bg-2022-135
Preprint. Discussion started: 29 June 2022
© Author(s) 2022. CC BY 4.0 License.


2 Methods

2.1 Study site and fieldwork description

The Kolyma River is the sixth largest river in the Arctic, with a watershed area of 653,000 km^2 (Holmes et al., 2012), that is completely underlain by continuous permafrost (Mann et al., 2012). Our area of study was a ~120 km section in the Kolyma River, bounded by the city of Chersky (68° 45' 5.1" N, 161° 18' 16.6" E) to the east and at the location known as Duvannyi Yar (68° 38' 12.8" N, 159° 5' 25.4" E) to the west (Fig. 1). Several floodplains are located next to the banks of this section of the Kolyma River. These floodplains connect the river to the land during the snow melt period (May and June) when they become inundated. We twice navigated the Kolyma River section onboard a small vessel (average navigation speed of 2.0±0.4 m s^{-1}), where we installed our instruments for measurements of continuous water properties and the partial pressure of methane (pCH$_4$) (Sect. 2.2.). The first transect was navigated in the upstream direction (UP) from Chersky to Duvannyi Yar (Fig. 1) between 15 June 2019 (12:48 h; local Chersky time) and 16 June 2019 (16:59 h) (with an overnight break halfway), covering a length of 127.7 km. The second transect was navigated in the downstream direction (DOWN) from Duvannyi Yar to Chersky, and took place between 16 June 2019 (17:00 h) and 17 June 2019 (13:27 h), covering a length of 115.4 km.

In 2019, the ice break-up in Kolyma River at Chersky started on 1 June, and our sampling took place during the late freshet. Thus, during the sampling campaign the transect navigated was completely ice-free and in the decreasing phase of the freshet peak discharge as shown by the daily records from the gauge station Kolymsk-1 (68° 43' 48" N, 158° 43' 12" E) in the Kolyma River (Fig. S1). During the sampling days, the average width of the Kolyma channel was about 2 km. With help of the Arctic DEM Explorer (Environmental Systems Research Institute, Polar Geospatial Center; https://livingatlas2.arcgis.com/arcticdemexplorer/), we estimated a total area of the sampled Kolyma River section of about 221 km^2.

Continuous water properties were measured along both transects (Sect. 2.2). The vessel primarily navigated at the center of the Kolyma River main channel during the sampling, particularly in the DOWN transect. We purposely navigated in the proximity of the confluences of tributaries and in banks adjacent to floodplains during the UP transect to capture the water properties in regions with visually evident, large lateral contributions from land (i.e., runoff from land as evidenced by more turbid and/or differently colored water).

To facilitate the analysis of the high-resolution data and analyze the specific contribution of banks and confluences with tributaries to the measured water properties and pCH$_4$, we defined five key sites (i.e., S1 to S5) that are associated with sampling points along the UP transect.

https://doi.org/10.5194/bg-2022-135
Preprint. Discussion started: 29 June 2022
© Author(s) 2022. CC BY 4.0 License.


From east to west the location of the "key sites" is: S1, bank of floodplain 1 at Ambolikha river in station PP07; S2, the confluence of tributaries Maly Anyuy and Bolshoy Anyuy (M&B Anyuy) in station PP11; S3, bank of floodplain 2 (only in DOWN transect) in station PP20; S4, bank of floodplain 3 (only in UP transect) in station PP23; and, S5, bank at Duvannyi Yar in station PP25 (Fig. 1). The separation between "key sites" and the "other sites" of the data was done on the basis of the measured pCH_4, T and κ in the UP and DOWN transects, and also analyzed independently for each transect.

The UP and DOWN transects were not navigated exactly at the same locations and the geographical overlap took place only in a few areas (Fig. 1). Therefore, we compare the results between these transects in the context of the temporal variability of the measured parameters, while the spatial variation is done between the key and other sites of the areas for each transect.

2.2 Collection of discrete river water samples and analysis

During the UP transect, we collected discrete water samples at 21 sampling stations (PP05-PP25) distributed along the track (see Fig. 1 for location and Table S1 for sampling times and average water properties measured at each station), for the analysis of dissolved organic carbon (DOC) and the composition of microbial communities (Sect. 2.3.). For this, a 1.5 L Niskin bottle was lowered to 1 m depth and water samples were drawn from the sampler onboard through silicone tubing.

2.2.1 Analysis of Dissolved Organic Carbon (DOC) in river water samples

For the quantification of DOC, a volume of 250 mL of water was transferred from the Niskin bottle into an acid-washed amber glass flask for quantification of DOC. The samples were stored at 4 °C until pre-treatment at the laboratory of the Northeast Science Station in Chersky after the sampling campaign. The samples were brought to room temperature and filtered through a pre-combusted 0.7 µm GF/F filter (Whatman®). Two aliquots of 10 mL of the filtrate for each sample were transferred to acid-washed glass vials and acidified to pH 2.0 with 37 % HCl. The samples were kept cold during storage and transport to Germany for the determination of DOC via high-temperature catalytic combustion (Analytik Jena), with each sample measured from three to five times as analytical replicates.

2.2.2 Analysis of microbial communities in river water samples

We determined the distribution and total community composition of microbial communities, including CH_4-producing archaea (methanogens) and CH_4-oxidizing bacteria (methanotrophs and methylotrophs) in the river water samples. Methanotrophs utilize CH_4 as carbon source, whereas methylotrophs are more versatile and can also use other C1 compounds as carbon

https://doi.org/10.5194/bg-2022-135
Preprint. Discussion started: 29 June 2022
© Author(s) 2022. CC BY 4.0 License.


source. In addition, the abundance of bacteria and archaea was determined along the transects. For this, a volume of 500 mL of the surface river water from the Niskin bottle was transferred into a 500 mL glass flask (DURAN® Borosilicate glass, SCHOTT). Using a hand pump and filtration system, this sample was immediately filtered on board through a 0.2 µm filter (Supor®). The 500 mL were divided into three aliquots and filtered independently for analytical replication. The filters were stored inside 2 mL sterile Biozym tubes and submerged in DNA/RNA shield solution (Zymo Research). The tubes with the filters remained at room temperature for their subsequent transport and analysis in Germany for DNA isolation, amplicon sequencing, and 16S rRNA gene quantification following protocols specified in the supplementing text S.1.2. and S.1.3.

2.3 Instrumental setup

Two instruments were installed onboard the vessel for continuous measurements of water properties: (1) an EXO2 multiparameter sonde with seven sensors for simultaneous optical and non-optical water measurements (Sect. 2.3.1), and (2) a Flow-Through (FT) system for continuous measurements of the partial pressure of CH_4 (pCH_4) (Sect. 2.3.2). The instruments were continuously fed with water pumped from the port side of the vessel from a nominal depth of 1 m below the water surface, hereinafter referred to as "surface water". The surface water was delivered through a PVC tubing of 2.5 m length and split into two outlets: 1) to feed the FT system at an approximate flow rate of 0.14 L s^{-1}, and 2) to a 20-L FT box located onboard where the EXO2 probe was immersed for the continuous surface water measurements.

2.3.1 EXO2 Sonde

The EXO2 multiparameter sonde (YSI Inc., Xylem Inc., Yellow Springs, OH, USA) was used to measure optically the turbidity (in formazin nephelometric units, FNU), dissolved O_2 (DO, µmol L^{-1}), and fluorescent dissolved organic matter (*f*DOM; Quinine Sulfate Units, QSU) of the incoming surface river water. It also measured temperature-corrected conductivity (specific conductivity, κ in µS cm^{-1}) with conductivity electrodes, water temperature (*T*, °C) with a thermistor, and pH with a glass electrode. The sonde had an internal battery and was mounted inside a metal frame (to provide protection and stability) submerged inside the 20 L FT box that received the incoming water pumped from the surface. The bucket was kept covered with a lid to avoid heating of the water and light exposure of the sensors. Considering the same water flow rate at the FT box as in the FT system, the water retention time in the FT box was on average 2.3 min, which allowed a sufficient time for the sensors in the probe to stabilize for a reliable measurement.

https://doi.org/10.5194/bg-2022-135
Preprint. Discussion started: 29 June 2022
© Author(s) 2022. CC BY 4.0 License.


The sonde was equipped with a wiper brush that was used routinely to clean the window of the sensors to avoid interferences due to fouling caused by the accumulation of deposits. The wiping periods were registered and removed from the data set. We obtained one measurement every 5 sec and the data was monitored and stored in a computer onboard.

As a result of the travel distance of the pumped water through the pipe (see Sect. S.1.1 for details), the water within the 20 L bucket on board was on average 0.6 °C warmer and with 1.2 mg L^{-1} higher DO content than the in-situ water at 1 m depth. Thus, the EXO2 sonde *T* and DO measurements were corrected by these mean values. All the sensors of the sonde were factory-calibrated previous to the measurements. Two-point calibrations were performed on-site to the DO and pH sensors and no analytical drift was observed before and after the measurements that would have required correction. The measured *f*DOM was temperature corrected to a reference of 25 °C (Downing et al., 2012; Watras et al., 2011), and further corrections due to the turbidity influence in the sensor response to light attenuation were done after Snyder et al. (2018).

2.3.2 Flow-through (FT) system

The FT system is a portable and versatile flow-through sensor set-up for continuous direct measurements of pCH_4 from surface water. We used a HydroC® CH_4 FT sensor based on tunable diode laser absorption spectroscopy (-4H-JENA engineering GmbH, Jena, Germany). A SBE45 thermosalinograph sensor (Sea-Bird Electronics, Bellevue, USA) was used to measure the temperature (T_{FT}, °C) and conductivity of the incoming water. The HydroC® CH_4 FT sensor was factory-calibrated before and after the measurement campaign. The calibration and validation of the data were done following Canning et al. (2021a). Drift and response time corrections were not applied because we assume sufficient exposure of the water to the sensor at the low sailing speeds. Because the relatively long response time of the CH_4 sensor (of the order of 20 min), the obtained data are significantly smoothed and therefore, the captured gradients and extreme values might not be precisely geographically located. However, the advantage of the high-spatial-resolution data allowed for a surface coverage that help identify high methane concentration areas. For more in-depth corrections see Canning et al. (2021a).

Besides the slow navigation speed, the average time spent at each sampling station was 7±13 min (minimum of 2 min and maximum of 8 min), which allowed for further equilibration times of the surface water at the sensors of the instruments, particularly at sites with high methane concentration.

We obtained one measurement every 5 sec and the data were monitored and stored on a

https://doi.org/10.5194/bg-2022-135
Preprint. Discussion started: 29 June 2022
© Author(s) 2022. CC BY 4.0 License.


computer onboard. The EXO2 sonde and FT system data were averaged to 1 min values. During the measurements, we also navigated inside smaller tributaries, one located at halfway along the transect length (named here as Leonid's stream), and another at the end of the DOWN transect, located along the Ambolikha River. Because the water properties measured in these streams are very contrasting to the properties in the main stem, we removed these sections from the full data, but still present the average values measured along those transects.

2.4 CH_4 flux calculation

To obtain the gas exchange across the water-air interface (i.e., flux density) it is necessary to calculate the gas transfer velocities k. Here we followed two methods to obtain k: 1) using a hydraulic model as a function of water velocity and discharge, and the river configuration (Raymond et al., 2012), and 2) using a parameterization as a function of wind speed (Wanninkhof, 2014). This was done in order to cover a range of values given the large uncertainties of k in rivers.

The hydraulic model that we used to calculate k, is a function of stream velocity (V, m s^{-1}), river slope (S, unitless), water discharge (Q, m^3 s^{-1}), and water depth (D, m) (empirical Eq. 7 in Raymond et al., 2012):

$$k\_R12 = 4725 \times (VS)^{0.86} \times Q^{-0.14} \times D^{0.66} \quad (1)$$

The average stream velocity for the transect (V=1.27±0.1 m s^{-1}) was calculated from the mean daily water discharge from 15 to 17 June 2019 as reported at the gauge station Kolymsk-1 (Q=13267±950 m^3 s^{-1}) divided by the mean cross-sectional area in the channel (A=10400±9721 m^2). A was calculated from the average river depth (D=5.2±4.9 m) times the river width (W fixed at 2000 m) at the sampling times. The slope S for the Kolyma River along the 120 km channel was 0.003 % considering the mean elevation of 4 m, obtained from the slope map in the Arctic DEM Explorer (Environmental Systems Research Institute, Polar Geospatial Center; https://livingatlas2.arcgis.com/arcticdemexplorer/). An uncertainty of up to 7.8 % is obtained in this calculation mostly due to the use of an average river depth for the calculation of the cross-sectional area and the stream velocity. The section of the Kolyma River can be in places as shallow as 1.7 m and as deep as 21.6 m, leading to faster water flows as the water column is shallow. However, larger uncertainties are expected due to the variation in Q along the stream, since the values used here are daily averages measured at once single site at the Kolymsk-1 gauge station.

The empirical wind speed parameterization is used to also calculate k, followed by Wanninkhof (2014):

https://doi.org/10.5194/bg-2022-135
Preprint. Discussion started: 29 June 2022
© Author(s) 2022. CC BY 4.0 License.


$$k\_W14 = 0.251 \times (u_{10})^2 \quad (2)$$

Were u_{10} (m s^{-1}) is the wind speed normalized to 10 m above the water surface, following Amorocho and Devries (1980), calculated from the wind velocities measured at a height of 6 m above ground at a nearby eddy tower during the sampling period (Castro-Morales et al., 2022).

The k_R12 from the hydraulic model and k_W14 from the wind parameterization were standardized to a constant temperature using the Schmidt number (Sc) for CO_2 and freshwater at 20 °C, i.e., Sc_{CO2}=600 (Wanninkhof, 1992), and the Sc of CH_4 (Sc_{CH4}) (Wanninkhof, 2014) following:

$$k_* = k\_ * \times \left(\frac{Sc_{CH4}}{Sc_{CO2}}\right)^{-0.5} \quad (3)$$

The water-to-air flux density of CH_4 (F, amount $area^{-1}$ $time^{-1}$) was obtained with the following function: $F_* = k_* \cdot (C_w - C_{eq})$, where k_* is the gas transfer velocity (length $time^{-1}$) of CH_4 at the in-situ T (Eq. 3) for R12 or W14 (Eq. 1 and 2). The water-side equilibrium concentration of CH_4 (C_{eq}, µmol L^{-1}) is subtracted from the measured bulk CH_4 concentration in the water (C_w, µmol L^{-1}). C_w was calculated from the Bunsen solubility coefficient (β, mol L^{-1} atm^{-1}) that is calculated as a function of temperature Weiss (1970), while C_{eq} was calculated following Wiesenburg and Guinasso (1979). The atmospheric $p$$CH_4$ (atm) was calculated following:

$$p = x(P - pH_2O) \quad (4)$$

where x is the dry air mole fraction of CH_4. P is the barometric pressure and $p$$H_2O$ is the saturation water vapor pressure at in-situ water temperature (both in atm). We used the global mean dry air mole fraction of 1858.8 ppb for CH_4 during June 2019 according to the Global Monitoring Laboratory, NOAA (Dlugokencky and Tans, 2019), and a standard barometric pressure of 1 atm.

2.5 Data analysis

2.5.1 Correlation between water $p$$CH_4$ and water parameters

To simplify the analysis for finding the relationship between the multiple water parameters measured along the transect and $p$$CH_4$, we calculated 1-min averages from the continuous measurements of T, κ, pH, DO, fDOM and $p$$CH_4$ at the location of the discrete sampling stations in the UP transect. We also included for this analysis the DOC concentrations from each station (average values are summarized in Table S1). In addition, we calculated the shortest distance from each station (z_{stas}) and of the navigated transects (z) to any of the river banks and considered this distance as another parameter relevant for the distribution of $p$$CH_4$

https://doi.org/10.5194/bg-2022-135
Preprint. Discussion started: 29 June 2022
© Author(s) 2022. CC BY 4.0 License.


in the river. The river banks along the navigated transects were digitized in Google Earth Pro®, and no other property was used to define the geographical location of these limits; hence, the river banks are fixed locations without temporal variation for the period of our sampling. We obtained z_{stas} and z from the shortest physical distance between the geographical positions of the sampling stations and of the UP and DOWN transects to any of the defined river banks. The river banks and limits of the transect define the polygonal area of interest for this study (Fig. S2).

To find the correlation between the 1-min averages of pCH_4 and the water properties, as well as the DOC at the sampling stations and z_{stas}, we performed a Pearson pairwise linear correlation analysis (p <0.1).

2.5.2 Random forest regression analysis for extrapolation of transect pCH_4 into a polygonal area of the river section as a function of T, κ and z

We estimated the pCH_4 at the sampling times in the entire river area of a polygon delimited by the river banks and the limits of the navigated transects (Fig. S2). The river bank-forming polygon of the Kolyma River section covered an area of 236.3 km^2. Within this area we constructed a fine grid regularly distributed within the river polygon and with a horizontal spatial resolution of 0.1 km.

We then built a fine grid polygon in the river for T and κ based on their best fit correlations to z at the transect scale, for the "key sites" and for the "other sites" (depending on the measured pCH_4, T and κ) at the sampling times during the UP and the DOWN transects. The gridded products were used to extrapolate pCH_4 to other areas of the river as defined by the gridded area delimited by the river banks, and on the basis of the highly spatially resolved pCH_4 measured along the transects.

For this, we obtained a best fit between T, κ and z to pCH_4 by applying a random forest regression analysis. First, for "key sites", this was done as a function of T and κ, i.e., $pCH_{4\_key}(T_{key}, \kappa_{key})$. Second, for "other sites" it was done as a function of T, κ and z, i.e., $pCH_{4\_other}(T_{other}, \kappa_{other}, z)$. These models were applied to the gridded polygon to extrapolate pCH_4 from the transects to the entire gridded polygon. Once a gridded T and κ was obtained, the corresponding model for pCH_{4_key} and pCH_{4_other} was applied. This procedure was done independently for the UP and DOWN data.

3 Results

3.1 Spatial distribution of continuous surface pCH_4 and water properties in UP and DOWN transects

The high-resolution continuous measurements of surface pCH_4 show significant spatial

https://doi.org/10.5194/bg-2022-135
Preprint. Discussion started: 29 June 2022
© Author(s) 2022. CC BY 4.0 License.


heterogeneity and temporal variability in both the UP and DOWN transects (Fig. 2). Overall, high pCH_4 (up to 46 µatm) was measured in the presence of warm (15.5 °C) and less conductive ($\kappa < 88$ µS cm^{-1}) water, and mostly located closer to the river banks ($z < 1.0$ km) (Figs. 3 and 4).

During the UP transect, the average measured pCH_4 was 25.8±6.7 µatm (or in terms of CH_4 concentration, $C_w = 41.5±9.2$ nmol L^{-1}). These values were measured in colder (by 0.6 °C) and less conductive waters (by 16.1 µS cm^{-1}) compared to the DOWN transect that was navigated two days later. The DOWN transect had on average 7.4 µatm higher pCH_4 (33.2±9.4 µatm, or 54.3±14.7 nmol L^{-1}) than the UP transect (Table 1 and Fig. 3). In both transects, the concentration of CH_4 remained supersaturated (by 1189±198 % in the UP transect and 1622±380 % in the DOWN transect) with respect to the concentration at atmospheric equilibrium (average 3.2±0.04 nmol L^{-1}).

The spatial distribution of water properties measured in both transects depicted evident differences between the center of the main stem and the areas at the proximity of banks adjacent to floodplains and at confluences of tributaries with the Kolyma main stem (Fig. 2a and 2b, and supplementary Fig. S3). Specifically, hot spots of pCH_4 with values > 35 µatm were measured in the key sites at the time of the measurements (Figs. 2 and 3).

During the UP transect, the maximum measured pCH_4 was 46.1 µatm at site S5 (Duvannyi Yar), very similar to the value measured during DOWN at the same location (i.e., 44.6 µatm). The maximum pCH_4 measured in the main stem (80.7 µatm) was found at a site halfway along the DOWN transect in a site at the outlet of Leonid's stream (location 68.5281 °N, 160.3437 °E). However, the highest pCH_4 was measured inside streams or tributaries with up to 222.9 µatm at Ambolikha River and up to 92.9 µatm inside Leonid's stream, both navigated during the DOWN transect (Table 1). Larger supersaturations with respect to the atmospheric equilibrium were observed at these two transects with 9610±403 % in Ambolikha River and 3415±1051 % in Leonid's stream.

In addition to pCH_4, T and κ were considered to distinguish between the key sites S1 to S5 from the other sites in the river. The key sites S1 to S5 were characterized (besides $pCH_4 > 37$ µatm) by the presence of warmer ($T > 14.5$ °C) and less conductive water ($\kappa < 88$ µS cm^{-1}) at the sampling time. Finally, because the key sites S1 to S5 were evidently located in the proximity of tributary confluences and banks (i.e., $z < 0.8$ km), we also considered z (distance to the river bank) as a parameter related to high pCH_4 in the main stem (Fig. S2 in supplement). The average, minimum and maximum values of pCH_4, C_w, T, and κ in the UP and DOWN transects at "key sites" and all "other sites" of the transect are summarized in

https://doi.org/10.5194/bg-2022-135
Preprint. Discussion started: 29 June 2022
© Author(s) 2022. CC BY 4.0 License.


Table 1.

Other areas along the transects where pCH_4 was higher than 37 µatm were not included as part of the key sites because their corresponding T or κ did not meet the properties specified above, e.g., at the site of the maximum pCH_4 of 80.7 µatm at the outlet of Leonid's stream where the T = 15.4 °C and κ = 113.1 µS cm^{-1} (Figs. 2 and 3).

The pairwise linear correlation analysis (p <0.1) between all the measured parameters showed a statistically significant positive correlation between pCH_4 and T (r^2 = 0.51), and a negative correlation to κ (r^2 = 0.22), z_{stas} (r^2 = 0.36), and DO (r^2 = 0.17). No significant correlation was found between pCH_4, fDOM and turbidity.

To analyze if any of the measured water parameters had an influence on the distribution of pCH_4, we chose the conservative tracers to which CH_4 was significantly correlated: T, κ, and z_{stas}. These conservative parameters are then considered as potential predictors for the presence of dissolved CH_4 in the river, in contrast to reactive tracers such as DO that can be biologically or chemically altered in the river water. The analysis of environmental indicators was done with the continuous high-resolution data only for the main stem areas.

3.2 Influence of conservative tracers on the distribution of riverine pCH_4 along transects and random forest regression as a gap-filling approach

The variations of T and κ in the river are influenced by the proximity to the outlets of tributaries and the riverbanks. This influence is more evident in the UP transect, where T and κ at "key sites" correlated positively with z (r^2 > 0.45, p = 0.05) (Fig. S4). In the data for the "other sites", the relation between T and κ vs. z, followed a semi-logarithmic fit (p = 0.05) in both the UP and DOWN transects (Fig. S5).

To be able to fill gaps and extrapolate the pCH_4 measured along the transects into the entire polygonal river area, we employed a random forest regression approach based on the correlations between T, κ and z. For this, we first built a fine-gridded polygon for T and κ using the linear (for "key sites") and semi-logarithmic correlations (for "other sites") observed at the transect level during the sampling times. Once a gridded T and κ were generated, the corresponding random forest model for pCH_{4_key} and pCH_{4_other} at transect level as a function of T, κ and z correspondingly, was applied. This procedure was done independently for the UP and DOWN transects, hence two polygons representing the modeled pCH_4 during 15–16 June 2019 and 16–17 June 2019 were obtained (Fig. S6).

To validate the output of the random forest models, we compared the measured and modeled pCH_4 along each transect. Results show that the skill of the model for the UP transect better reproduces the pCH_4 with an uncertainty of 3.9 µatm than that of the model for the DOWN

https://doi.org/10.5194/bg-2022-135
Preprint. Discussion started: 29 June 2022
© Author(s) 2022. CC BY 4.0 License.


transect (uncertainty of 9.1 µatm) (Fig. S7). A larger error is observed in the areas of the key sites mostly during the DOWN transect.

3.3 Microbial composition and DOC analysis in discrete water samples

Similar to the influences of temperature (T) and specific conductivity (κ) on the distribution of pCH_4, we found that microbial community composition was significantly related to both T ($F = 15.5$, $r^2 = 0.17$, $p < 0.001$) and specific conductivity (κ) ($F = 12.7$, $r^2 = 0.14$, $p < 0.001$) (Fig. 5), while distance to the shore (z) was not significant. The pCH_4 measurements alone explained a low portion of the community variance ($r^2 = 0.06$, $p < 0.03$), and when tested in conjunction with both T and κ, was not a significant contributor to microbial community variance. In this way, microbial community composition can act as a record of pCH_4, as microbes – and T/κ – are less dynamic than pCH_4. Within the context of the strong patterns related to both T and κ, there were spatial patterns that reflected the location within the main stem and the influences of tributaries, with key site S3 (PP20) exhibiting the lowest similarities with the other four key sites and clustering with other water samples collected within the main stem of the river. Conversely, key sites S1 and S2 clustered separately from all other water samples, likely due to the heavy influence of tributary outflow and floodplain inputs (Fig. 5).

Quantifying the 16S rRNA gene abundances of total archaeal and bacterial populations revealed that archaea, were three orders of magnitude lower in abundance than their bacterial counterparts across the river transect. However, the abundances of both were found to strongly correlate (Pearson, $r^2 = 0.81$, $p < 1.8e{-}15$) (Supplemental Fig. S8). Within the archaeal 16S sequences detected, we found two putatively methanogenic OTU, each belonging to a different family/genus (*Methanobacteriaceae – Methanobacterium, Methanoregulaceae – Methanoregula*). The highest relative abundance of methanogens (0.012 %) occurred within station PP07 (key site S1) (Fig. 6a), and the other key sites with the highest CH_4 concentrations did not exhibit particularly elevated methanogens abundances. Conversely, bacterial putative groups associated with methanotrophy/methylotrophy, particularly OTU within the family *Methylophilaceae*, were detected at all sites and ranged between 3.5 to 5.5 % relative abundance (Fig. 6b). Restricting our analysis to genera known to be strict methanotrophs, we find sequences affiliated with *Methylobacter* that range from 0.01 – 0.3 % relative abundance, and only traces of *Ca.* Methanoperedens (Supplemental Fig. S9). The relative abundances of these groups were approximated to pseudo-absolute abundances using the quantitative qPCR results from each sample. Patterns in methanogen abundances were consistent regardless of scale (Fig. 6c), while methano-/methylotrophs

https://doi.org/10.5194/bg-2022-135
Preprint. Discussion started: 29 June 2022
© Author(s) 2022. CC BY 4.0 License.


exhibited higher abundances within stations PP10, PP11 (key site S2), and PP23-PP25 (incl. key sites S4 and S5), and lower abundances within PP06, PP09, PP15, PP17, and PP20 (key site S3) (Fig. 6d).

The correlations between the total absolute abundances of archaeal microbial communities against the water properties at stations (Fig. 7) show a positive linear correlation between T and the abundance of methanogens (r^2=0.35, p = 0.05) and methano-/methylotrophs (r^2=0.43) (Figs. 7a and 7b). A negative linear correlation against κ (r^2=0.31 for methanogens and r^2=0.24 for methano-/methylotrophs) (Figs. 7c and 7d). The pCH$_4$ at stations is also positively correlated to the abundance of methanogens (r^2=0.11) and methano-/methylotrophs (r^2=0.21) (Figs. 7e and 7f).

The average DOC measured in all of the sampling stations was 9.0±1.0 mg L^{-1}. The largest DOC values were measured at some of the sampling stations located on the east side of the transect at the confluence between tributaries and the Kolyma main stem or closer to the river bank. The highest measured DOC value was 11.9 mg L^{-1} at station PP05, located at the confluence between the Panteleikha-Ambolikha rivers and the Kolyma main stem, whereas the lowest DOC value was measured at station PP25 near the river bank at Duvannyi Yar (7.5 mg L^{-1}) despite the large turbidity observed in this site. Other sampling stations located at confluences or near banks reached values ≥ 9 mg L^{-1}, i.e., PP07 and PP10 close to the riverbank, PP18 and PP19 located inside and outside Leonid's stream respectively, as well as station PP11 at the confluence to the Maly and Bolschoi Anjui (M&B Anjui) tributaries (Table S1 and Fig. S10). No significant correlation ($p < 0.1$) was found between pCH$_4$ and DOC.

3.4 Surface CH$_4$ emissions at transects and polygonal surface area at the Kolyma River section

The average gas transfer velocity during the sampling period was calculated with a hydraulic model (k_{R12}=0.5±0.02 m d^{-1}) and a wind speed parameterization (k_{W14}=0.4±0.3 m d^{-1}) are in close agreement. Because the magnitude of the flux density of CH$_4$ calculated in both transects with these two k values does not differ considerably (i.e., F_{R12}=0.02±0.007 mmol m^{-2} d^{-1} and F_{W14}=0.01±0.01 mmol m^{-2} d^{-1}), we chose to present only F_{R12} calculated using k_{R12} after the hydraulic model. F_{R12} will be presented hereinafter to as the flux density of CH$_4$, FCH$_4$.

The average FCH$_4$ of CH$_4$ along the UP transect was 0.019±0.005 mmol m^{-2} d^{-1} and along the DOWN transect was 0.026±0.008 mmol m^{-2} d^{-1}. Maximum FCH$_4$ values at key sites were 0.034 mmol m^{-2} d^{-1} for site S5 during the UP transect, and 0.045 mmol m^{-2} d^{-1} at the key site

https://doi.org/10.5194/bg-2022-135
Preprint. Discussion started: 29 June 2022
© Author(s) 2022. CC BY 4.0 License.


S2 during the DOWN transect (Fig. 3). Average FCH_4 in both transects was 1.5 times higher at key sites than in the other sites of the transects (Fig. 7). This is relevant considering that the surface area represented by the key sites is 8 to 12 times smaller than the rest of the transects (calculated considering the navigated distance times a radius of 50 m around the sampling point).

The cumulative sum of the CH_4 fluxes in the UP transect for the period of sampling (1 day) was 14.4 mmol m^{-2}. At key sites, the fluxes accounted for 13 % (1.8 mmol m^{-2}) of the total flux. In the DOWN transect, the total CH4 flux was 10.5 mmol m^{-2}, and the contribution of the key sites to the total emissions increased to 20 % (2.1 mmol m^{-2}).

We also calculated FCH_4 for a smaller stream (Leonid's stream) and the Ambolikha River (second-order tributary of Kolyma River) (Fig. 1), that were navigated during the DOWN transect on 17 June 2019. These navigated sections were not included in our estimate for main channel. The average FCH_4 at the Ambolikha River (0.17±0.008 mmol m^{-2} d^{-1}) and at the Leonid's stream (0.05±0.02 mmol m^{-2} d^{-1}) were nearly five and two times higher respectively than at the key sites of the main channel during the DOWN transect (Fig. 7).

Based on the modeled pCH_4 in the gridded surface area of the Kolyma River section, we calculated the corresponding FCH_4 that would have been emitted through the total surface of the river section (236.3 km^2). The total CH_4 flux at the surface of the river section during the UP transect is calculated as 934.2 mmol d^{-1} (or 1.1×10^4 mgC d^{-1}), and for the DOWN transect is 1391.9 mmol d^{-1} (or 1.7×10^{14} mgC d^{-1}). This estimation allows for the calculation of the flux of gas through the entire surface area of the river section (and not only at the transect locations). We estimated an average of 3.3×10^{12} mgC d^{-1} (equivalent to 3300 tC d^{-1}) of the total CH_4 emitted through the surface of the Kolyma River section during the sampling time of both transects (15-17 June 2019).

4 Discussion

4.1 Patterns and indicators of the spatial distribution of methane in Kolyma River and associated tributaries and streams

In June 2019, the Kolyma River exhibited large pCH_4 values that were up to 1,300 % supersaturated (equivalent to 28.3±8.5 µatm) with respect to atmospheric equilibrium. These values are comparable to measurements reported for summer in the main channel of the Lena River, i.e., 18 to 51 µatm, calculated from 30 to 85 nmol L^{-1} for a T=14 °C in freshwater; (Bussmann, 2013). However, a large range in pCH_4 values has been measured in other Arctic Rivers, such that the average pCH_4 in the Kolyma River is three times higher than measurements at the main channel of the Yukon River in North America (8.4 µatm) (Striegl

https://doi.org/10.5194/bg-2022-135
Preprint. Discussion started: 29 June 2022
© Author(s) 2022. CC BY 4.0 License.


et al., 2012), and almost nine times lower than the mean pCH_4 value (236 µatm) in surface waters of Kuparuk River in Alaska (Kling et al., 1992).

Our highly spatially-resolved underway continuous measurements of surface dissolved CH_4 were pivotal to reveal spatial variabilities and features in the main river channel that cannot be obtained with sparse discrete sampling. The surface distribution of pCH_4 measured in a ~120 km section of Kolyma River was heterogeneous, with nearly two-fold higher concentrations observed along riverbanks and near the confluence of tributaries (69 nmol L^{-1}, or pCH_4=41.1 µatm) than at the central parts of the river (46 nmol L^{-1}, or pCH_4=27.8 µatm) (Fig. 2 and Table 1). Previous studies have demonstrated the influence of land to the distribution of riverine CH_4 concentrations, for example along the Danube River (Canning et al., 2021b), and within the Lena River (Bussmann, 2013). The concentration of dissolved CH_4 in Arctic sites with direct contact to adjacent lands, such as in small tributaries, streams, lakes channels or ponds, has been shown to be two to five times higher than what is observed in the main stems of large rivers (Bussmann, 2013; Dean et al., 2020; Kling et al., 1992; Striegl et al., 2012). In samples from creeks draining from permafrost into the Lena River, CH_4 concentrations (1505 nmol L^{-1}, or pCH_4 of 900 µatm) were between twenty to fifty times higher than in fluvial waters (Bussmann, 2013). At the Lena Delta, the concentrations of CH_4 are higher (212 nmol L^{-1}, or pCH_4 of 114.7 µatm, T=9.8°C and S=2.45), because they were directly influenced by bottom soils (Bussmann et al., 2017). In tributaries of the Yukon River, the CH_4 concentrations were up to 690 nmol L^{-1}, being two times higher than in the main stem of the same river (290 nmol L^{-1}) (Striegl et al., 2012). Similarly, our results show that, besides the in-stream variability, tributary or stream CH_4 concentrations measured at the Ambolikha River and Leonid's stream, were between two to six times higher than those in the main channel of Kolyma River.

The average pCH_4 measured at the Ambolikha River (206.8±9.8 µatm) is consistent with the measurements at the Kuparuk River (236 µatm) (Striegl et al., 2012), and the mean pCH_4 (292±109 µatm) measured during a 38-day time-series study that started 9 days after the present study (i.e., on 26 June 2019) at a site in the Ambolikha River (Castro-Morales et al., 2022). Whereas the average CH_4 concentration measured at Leonid's stream was 67 µatm (111 nM), which is in the same order of magnitude as the maximum value measured at the plume of Kolyma River at the East Siberian Arctic shelf in the summer of 2004 (55 µatm, obtained from the reported 110 nM, T=5 °C and S=14) (Shakhova and Semiletov, 2007).

We characterized the spatial distribution of riverine pCH_4 as a function of temperature (T), specific conductivity (κ) and the distance from the river banks (z), as suitable indicators for

https://doi.org/10.5194/bg-2022-135
Preprint. Discussion started: 29 June 2022
© Author(s) 2022. CC BY 4.0 License.


the distribution of CH_4 during the late spring over larger areas of the Kolyma River (and potentially applicable to other Arctic rivers). We found that the distance to river banks is an indicator of the proximity to potential terrestrial CH_4 sources, hence it can be a useful benchmark for understanding the distribution and fate of CH_4 in natural surface waters (Fig. 4). With a statistical approach, we used the selected predictors to fill gaps in areas of the river where no CH_4 data were available (Fig. S6). Similar approaches could be used to improve the CH_4 data currently available for the global CH_4 budget (Saunois et al., 2020) and to aid in forecasting riverine CH_4 following the projected increases in warmer river waters, abrupt permafrost thawing, and collapse of riverbanks.

4.2 Identification of microbial communities associated with the riverine CH_4 concentrations

Overall patterns in microbial community composition, e.g., the similarities in the relative abundances of bacterial and archaeal groups, were also strongly related to the temperature and specific conductivity of the river water (Fig. 5). Unlike with CH_4, distance to shore was not apparent in explaining differences in community composition. Arctic riverine microbial communities track closely with water temperature, flow rate, and biogeochemistry (Campeau and del Giorgio, 2014; Crump et al., 2009) and match patterns in DOM composition and concentration (Castro-Morales et al., 2022; Kaiser et al., 2017). The strong explanatory power of temperature and specific conductivity we observe in this study fits in with the concept of riverine community coalescence as they approximate the mixing of distinct water sources over a spatially small region, whereby the dynamic community assemblage mechanisms are inextricably linked to transport processes and rapidly changing selective pressures (Mansour et al., 2018). In this sense, spatial patterns in community composition can act as robust bioindicators of the relative inputs of transported metabolic end products derived from terrestrial sources, like CH_4 or CO_2. To support the relationship between community composition and the originating source of CH_4, we examined the distributions of functional microbial groups putatively associated with CH_4 production and consumption. The strongest evidence was the overlap in detected methanotrophs and methanogens within our study and a previous study by Kwon et al. (2017), that examined these groups within permafrost soils adjacent to our site (PP09). More specifically the highest relative abundances of groups associated with *Methanobacterium* and *Methylobacter* in both the surficial soils and our discrete water samples.

Expanding on this, biological CH_4 production is only known from the Archaeal domain of life, and methanogens, as strict anaerobes (Evans et al., 2019), are unsuited to grow within

https://doi.org/10.5194/bg-2022-135
Preprint. Discussion started: 29 June 2022
© Author(s) 2022. CC BY 4.0 License.


585 oxic river waters. We suggest that the relative and pseudo-absolute abundances of sequences affiliated with methanogens further act as more specific indicators of sources originating from anoxic, terrestrial CH_4 hotspots, as supported by the statistically significant correlation between methanogen abundance and methane concentration (Fig. 7). Additionally, we anticipate that the methanogenic archaea exhibit longer residence times than CH_4 itself due to
590 its high diffusion and oxidation rates. The presence of soil-derived methanogens in the river water might be indicative of even higher riverine CH_4 concentrations, as part of it can be already outgassed or oxidized. The weaker correlation of methane to methanogen abundance compared to temperature or specific conductivity, parameters expected to change slower than methane concentrations, likely reflects these differences in transport mechanisms. Of the two
595 methanogens we detected, *Methanobacterium* was recently shown to be the primary methanogen detected in the surface waters of thermokarst ponds and is more typical of acidic and peat-dominated aquatic ecosystems (Vigneron et al., 2019). *Methanoregula* (within order *Methanomicrobiales*) have also been shown to be abundant groups within permafrost thaw lakes (Crevecoeur et al., 2016) and were suggested to be more typical of deeper and less
600 acidic water bodies (Vigneron et al., 2019) (Fig. 6).

Conversely, we expected microbial groups that consume CH_4 to also be indicative of CH_4 sources into the river. Groups affiliated with methylotrophy (e.g., *Methylophilaceae – Methylotenera*) exhibited ten times higher relative abundances than groups of strict methanotrophic organisms (*Methylobacter*) (Fig. 6), suggesting that in addition to methane,
605 other sources like methanol associated to the degradation of CO_2 by methanotrophs (Xin et al., 2007) or by some groups of phytoplankton (Mincer and Aicher, 2016), were sources of carbon in this environment. In support of this finding, aerobic methanotrophs have been found at much higher relative abundances (>25 %) and higher diversity within thermokarst well-stratified subarctic Canadian ponds, than the maximum of 0.3 % detected here, where distinct
610 genera (Methylobacter and Methylomonas) within the order *Methylococcales* where the most abundant (Crevecoeur et al., 2015; Vigneron et al., 2019). This is a sensical finding, as the dynamic river flow enables the diffusive methane transport and emissions to the atmosphere compared to the emissions across smaller surface areas in highly-stratified, less dynamic and largely anoxic pond environments. The majority of the CH_4 produced in thawing permafrost
615 is first locally oxidized before it can be released to the atmosphere (Olid et al., 2021). Thus, the higher relative abundance of CH_4-consuming bacteria compared to CH_4-producing archaea in the Kolyma River suggests that a considerable fraction of CH_4 is already oxidized within the recently thawed active layer.

https://doi.org/10.5194/bg-2022-135
Preprint. Discussion started: 29 June 2022
© Author(s) 2022. CC BY 4.0 License.


4.3 Temporal variability of methane in Kolyma River

Our continuous high-resolution measurements of pCH_4 in the Kolyma River allowed us also to identify a large temporal variability in spite of the short time scale of our measurements. The differences in the pCH_4 and FCH_4 (flux density of methane) between the UP and DOWN transects might be due to a rapid response to changes in CH_4 driven by the interactions between the main flow of the river and the continuous contribution of external CH_4 inputs resulting from melting, rather than by an advective signal travelling down the main channel of Kolyma River. Still, our measurements cannot represent any mid- to long-term CH_4 variation in the river, and the differences between the transects might also be due to different spatial locations.

The Kolyma River Basin is the only one in the Arctic completely underlain by continuous permafrost, which could result in even higher soil CH_4 production and release into the river network during permafrost thaw compared to other Arctic rivers. During the Arctic melt season (May to June), the surface hydrologic connectivity between the land and rivers is enhanced. As the seasonal progression takes place, deeper water-saturated soil layers are thawed, and substances, microorganisms, and gases, like CH_4, are mobilized through the lateral transfer from groundwater discharge into Arctic inland waters, particularly to the fluvial network (Connolly et al., 2020; Harms et al., 2020; Saunois et al., 2020). It has been demonstrated that the majority of the CH_4 emitted to the atmosphere from subarctic ponds is sustained by the discharge of CH_4 from groundwaters upon the active layer thaw (Olid et al., 2021).

4.4 Methane emissions in Kolyma River and comparison to other estimates

The average estimated annual flux in the polygon section at the Kolyma River during our sampling is 0.63×10^{12} g CH_4 yr^{-1} (or 0.63 Tg CH_4 yr^{-1}, for a 146-days ice-free season between 20th May and 12th October 2019 obtained from the river discharge curve, Fig. S1) considering a surface area of 236.3 km^2. These emissions are on the same order of magnitude as the annual flux of CH_4 at the East Siberian Arctic Shelf (ESAS) estimated to be 0.11×10^{12} g CH_4 yr^{-1} (or 0.11 Tg CH_4 yr^{-1}, for a 90-days ice-free season) in summer of 2003 and 2004 for a surface area of 1.0×10^6 km^2 (which is orders of magnitude greater than the polygon section of Kolyma River) (Shakhova and Semiletov, 2007). In Arctic shelves, the concentration of CH_4 is strongly influenced by riverine inputs, particularly in to bottom layers of shelf waters due to differential water density gradients (Shakhova and Semiletov, 2007). Decreasing flow velocities (i.e., discharge) allow sedimentation of organic matter in the delta areas, stimulating microbial sedimentary processes that finally lead to the formation of CH_4

https://doi.org/10.5194/bg-2022-135
Preprint. Discussion started: 29 June 2022
© Author(s) 2022. CC BY 4.0 License.


and CO_2. Dropping water levels during summer also facilitates CH_4 emissions from riverine sediments to the atmosphere. This has been observed in the Lena River region, where contributions from bottom surface sediments are more significant to the measured CH_4 concentrations than riverine lateral exports (Bussmann et al., 2017).

Taking into account a polygon surface area of 236.3 km^2 and 146 days of ice-free water, we estimated a total flux of 0.63 Tg CH_4 yr^{-1} in the investigated river section. This calculation is by far robust and largely uncertain, considering that our measurements only correspond to a short-term data set during the open water season, and that large temporal and spatial variations in relation to e.g., changes in water sources, temperature regime and lateral carbon inputs throughout the ice-free period is expected. This has been recently demonstrated at the Ambolikha River (tributary of the Kolyma River), where riverine CH_4 concentrations decreased over time during the open water season due to persistent emissions to the atmosphere dominating over declining external gas inputs during the summer low flow (Castro-Morales et al., 2022). Still, the annual CH_4 flux value provided here for the investigated Kolyma River section, provides an upper end of the potential magnitude and relevance of CH_4 atmospheric emissions from an Arctic River.

As both the oxidation rates and the diffusive emissions of CH_4 through the water-atmosphere interface are faster processes than the lateral gas transport in the water column. Thus, despite the large CH_4 concentrations and emissions identified in the upstream river waters, the surface riverine CH_4 measured >100 km upstream of the shelf is locally emitted (or oxidized) and does not influence the surface CH_4 concentrations measured at the river plume and at the East Siberian Arctic Shelf.

Morphology and stream size seem to be also key parameters for the amount of gas delivered from land and emitted through the water surface into the atmosphere, as the potential for large gas emissions is higher in smaller streams with shorter water travel distances. Our data support this assumption, as the FCH_4 at key sites was two to five times lower than the average FCH_4 at the smaller Leonid's stream and Ambolikha River respectively (Fig. 8). The surface areas of the key sites characterized by elevated FCH_4 are between 8 to 12 times smaller than the surface area covered by the rest of the transect. However, the CH_4 emissions at key sites were 1.5 times higher than in the other sites, and represent between 13 to 20 % of the total cumulative emissions in both transects.

Because the diffusion of CH_4 in water is slower than in air, riverbanks can thus act as efficient vectors for the local emissions of CH_4 formed and stored in the subsoil. The projected increase in freshwater inputs, deepening of active layers, and increase in soil drainage, as

https://doi.org/10.5194/bg-2022-135
Preprint. Discussion started: 29 June 2022
© Author(s) 2022. CC BY 4.0 License.


more permafrost is thawing in response to warmer and wetter Arctic summers (AMAP, 2017; Bring et al., 2016; Bussmann et al., 2017; Chiasson-Poirier et al., 2020), will enhance the input of CH_4 from external terrestrial sources at hotspots over extended periods during the open water season. Additionally, projected longer ice-free periods in the Arctic, i.e., an earlier start of melt periods and longer open water seasons, can therefore lead to an increase in CH_4 emissions from inland waters (Wik et al., 2016). This ultimately will have an impact on the current CH_4 budget of the Arctic. By not considering the variable aquatic ecosystems and water cycle of the Arctic, the estimated 4 to 5 % contribution of high latitudes to the total global methane emissions (Rosentreter et al., 2021; Saunois et al., 2020) may be underestimated.

The irregular location of CH_4 hot spots along the river banks and their potentially continuous elevated CH_4 contributions to the river, possess a challenge to estimating lateral transport of CH_4 from upstream to downstream waters. Elevated CH_4 concentrations at the Arctic shelves are thus primarily influenced by local sources (i.e., bottom soils and degrading shelves) (Shakhova and Semiletov, 2007). However, to improve the estimates of riverine CH_4 concentrations that can actually reach the ocean in the context of increasing warming and thawing, and to improve the knowledge of the contribution of Arctic rivers and streams to the regional and global CH_4 budgets, it is necessary to intensify the spatial and temporal resolution of the direct measurements of CH_4 in Arctic Rivers.

5 Conclusions

In this study, we measured for the first time continuous high-resolution pCH_4 in a large section of Kolyma River during the late freshet of 2019, and combined these observations with microbial community analysis in water samples to investigate the potential source of this gas. The large spatial variability of surface methane concentrations in the river channel was associated with hotspots located at the river bank and at confluences with tributaries where methane was almost two times higher than at the center of the channel. The identified presence of methane-producing archaea in a well oxygenated river water suggests that most of the CH_4 is laterally transported from external terrestrial sources into the river channel, rather than produced within the river water. Elevated riverine local methane emissions were associated with identified hotspot areas on land suggesting efficient linkages between the land and the aquatic ecosystems. Upstream river boundaries do not seem to be a source of CH_4 into the Arctic Ocean via downstream transport with the river flow. Without continuous measurements, it will remain unclear how much CH_4 is actually transported and emitted at the peak of the melt period at the highest annual river discharge. Certainly, more abrupt collapses,

https://doi.org/10.5194/bg-2022-135
Preprint. Discussion started: 29 June 2022
© Author(s) 2022. CC BY 4.0 License.


erosion and thawing of the Arctic Ocean shelves may contribute to the liberation and transport of soil-derived CH_4 into the ocean, as well as subsequent emissions into the atmosphere. Our results provide a glimpse of the potential contribution of methane emissions from Arctic Rivers, adding up to the largely unknown contributions from permafrost and inland waters.

Data availability

The data presented in this work will be made available through a link to the Zenodo public repository upon the publication of this work.

Competing interests

The authors declare that they have no conflict of interest

Author contribution

K.C.-M. conceived and designed the study. K.C.-M, A.C., A.K., K.K., S.A., O.K. and N.Z. contributed to fieldwork and logistics. K.C.-M, A.C., M.G., S.A., W.A.O. contributed to lab work, sample and data analyses. K.C.-M., A.C. and W.A.O wrote the paper with contributions from all authors in draft versions prior to submission.

Acknowledgments

This work was conceived within the project PROPERAQUA funded by the Deutsche Forschungsgemeinschaft (DFG, German Research Foundation) (project No. 396657413). The contributions from AC and AK were funded by the MOSES program of the Helmholtz Association and the C-CASCADES ITN of the EU (project No. 643052). KK and WAO were supported by the Collaborative Research Centre 1076 AquaDiva (CRC AquaDiva) funded by DFG (project No. ID 218627073). MG and OK were supported through funding by the European Commission (INTAROS project, H2020-BG-09-2016, Grant Agreement No. 727890, Nunataryuk project, H2020-BG-11-2016/17, Grant Agreement No. 773421). Especial thanks to the Northeast Scientific Station and the Pleistocene Park in Chersky for their invaluable assistance during fieldwork. Thanks to Dr. Robert Lehmann for the analysis of DOC samples at the FSU-Jena.

https://doi.org/10.5194/bg-2022-135
Preprint. Discussion started: 29 June 2022
© Author(s) 2022. CC BY 4.0 License.

References

AMAP, Snow, water, ice and permafrost in the Arctic (SWIPA), In, Oslo, Norway, 269, 2017.

Amorocho, J. and Devries, J. J.: A new evaluation of the wind stress coefficient over water surfaces, Journal of Geophysical Research, 85, 433-442, 10.1029/JC085iC01p00433, 1980.

Bring, A., Fedorova, I., Dibike, Y., Hinzman, L., Mård, J., Mernild, S. H., Prowse, T. D., Semenova, O., Stuefer, S. L., and Woo, M.-K.: Arctic terrestrial hydrology: a synthesis of processes, regional effects, and research challenges, Journal of Geophysical Research: Biogeosciences, 121, 621-649, 10.1002/2015JG003131, 2016.

Bussmann, I.: Distribution of methane in the Lena Delta and Buor-Khaya Bay, Russia, Biogeosciences, 10, 4641-4652, 10.5194/bg-10-4641-2013, 2013.

Bussmann, I., Hackbusch, S., Schaal, P., and Wichels, A.: Methane distribution and oxidation around the Lena Delta in summer 2013, Biogeosciences, 14, 4985-5002, 10.5194/bg-14-4985-2017, 2017.

Campeau, A. and del Giorgio, P. A.: Patterns in CH_4 and CO_2 concentrations across boreal rivers: major drivers and implications for fluvial greenhouse emissions under climate change scenarios, Global Change Biology, 20, 1075-1088, 10.1111/gcb.12479, 2014.

Canning, A., Körtzinger, A., Fietzek, P., and Rehder, G.: Technical note: seamless gas measurements across Land-Ocean Aquatic Continuum - corrections and evaluation of sensor data for CO_2, CH_4 and O_2 from field deployments in contrasting environments, Biogeosciences, 18, 1351-1373, 10.5194/bg-18-1351-2021, 2021a.

Canning, A., Wehrli, B., and Körtzinger, A.: Methane in the Danube Delta: the importance of spatial patterns and diel cycles for atmospheric emissions estimates, Biogeosciences, 18, 3961-3979, 10.5194/bg-18-3961-2021, 2021b.

Castro-Morales, K., Canning, A., Körtzinger, A., Göckede, M., Küsel, K., Overholt, W. A., Wichard, T., Redlich, S., Arzberger, S., Kolle, O., and Zimov, N.: Effects of reversal of water flow in an Arctic stream on fluvial emissions of CO_2 and CH_4, Journal of Geophysical Research: Biogeosciences, 127, e2021JG006485, 10.1029/2021JG006485, 2022.

Charkin, A. N., M., R. v. d. L., Shakhova, N. E., Gustafsson, Ö., Dudarev, O. V., Cherepnev, M. S., Salyuk, A. N., Koshurnikov, A. V., Spivak, E. A., Gunar, A. Y., Ruban, A. S., and Semiletov, I. P.: Discovery and characterization of submarine groundwater discharge in the Siberian Arctic seas: a case study in the Buor-Khaya Gulf, Laptev Sea, The Cryosphere, 11, 2305-2327, 10.5194/tc-11-2305-2017, 2017.

Chiasson-Poirier, G., Franssen, J., Lafrenière, M. J., Fortier, D., and Lamoureux, S. F.: Seasonal evolution of active layer thaw depth and hillslope-stream connectivity in a permafrost watershed, Water Resources Research, 56, 10.1029/2019WR025828, 2020.

Connolly, C. T., Cardenas, M. B., Burkart, G. A., Spencer, R. G. M., and McClelland, J. W.: Groundwater as a major source of dissolved organic matter to Arctic coastal waters, Nature Communications, 11, 1-8, 10.1038/s41467-020-15250-8, 2020.

Crevecoeur, S., Vincent, W. F., Comte, J., and Lovejoy, C.: Bacterial community structure

https://doi.org/10.5194/bg-2022-135
Preprint. Discussion started: 29 June 2022
© Author(s) 2022. CC BY 4.0 License.

across environmental gradients in perfmafrost thaw ponds: methanotroph-rich ecosystems, Frontiers in Microbiology, 6, 192, 10.3389/fmicb.2015.00192, 2015.

Crevecoeur, S., Vincent, W. F., and Lovejoy, C.: Environmental selection of planktonic methanogens in permafrost thaw ponds, Scientific Reports, 6, 31312, 10.1038/srep31312, 2016.

Crump, B. C., Peterson, B. J., Raymond, P. A., Amon, R. M. W., Rinehart, A., McClelland, J. W., and Holmes, R. M.: Circumpolar synchrony in big river bacterioplankton, Proceedings of the National Academy of Sciences of the United States of America, 106, 10.1073/pnas.0906149106, 2009.

Dabrowski, J. S., Charette, M. A., Mann, P. J., Ludwig, S. M., Natali, S. M., Holmes, R. M., Schade, J. D., Powell, M., and Henderson, P. B.: Using radon to quantify groundwater discharge and methane fluxes to a shallow, tundra lake on the Yukon Kuskokwim Delta, Alaska, Biogeochemistry, 148, 69-89, 10.1007/s10533-020-00647-w, 2020.

Dean, J. F., Meisel, O. H., Martyn, R. M., Belelli, L. M., Garnett, M. H., Lenderink, H., van Logtestijn, R., Borges, A. V., Bouillon, S., Lambert, T., Röckmann, T., Maximov, T., Petrov, R., Karsanaev, S., Aerts, R., van Huissteden, J., Vonk, J. E., and Dolman, A. J.: East Siberian Arctic inland waters emit mostly contemporary carbon, Nature Communications, 11, 1627, 10.1038/s41467-020-15511-6, 2020.

Dean, J. F., Middelburg, J. J., Röckmann, T., Aerts, R., Blauw, L. G., Egger, M., Jetten, M. S. M., de Jong, A. E. E., Meisel, O. H., Rasigraf, O., Slomp, C. P., in't Zandt, M. H., and Dolman, A. J.: Methane feedbacks to the global climate system in a warmer world, Reviews of Geophysics, 56, 1-44, 10.1002/2017RG000559, 2018.

Dlugokencky, E. and Tans, P. P.: www.esrl.noaa.gov/gmd/ccgg/trends/, 2020.

Downing, B. D., Pellerin, B. A., Bergamaschi, B. A., Saraceno, J. F., and Kraus, T. E. C.: Seeing the light: the effects of particles, dissolved materials, and temperature on in situ measurements of DOM fluorescence in rivers and streams, Limnology and Oceanography: Methods, 10, 767-775, 10.4319/lom.2012.10.767, 2012.

Etminan, M., Myhre, G., Highwood, E. J., and Shine, K. P.: Radiative forcing of carbon dioxide, methane, and nitrous oxide: a significant revision of the methane radiative forcing, Geophysical Research Letters, 43, 12614-12623, 10.1002/2016GL071930, 2016.

Evans, P. N., Boyd, J. A., Leu, A. O., Woodcroft, B. J., Parks, D. H., Hugenholtz, P., and Tyson, G. W.: An evolving view of methane metabolism in the Archaea, Nature Reviews Microbiology, 17, 219-232, 10.1038/s41579-018-0136-7, 2019.

Harms, T. K., Rocher-Ros, G., and Goodsey, S. E.: Emission of greenhouse gases from water tracks draining Arctic hillslopes, Journal of Geophysical Research: Biogeosciences, 125, e2020JG005889, 10.1029/2020JG005889, 2020.

IPCC, Climate Change 2014: Synthesis Report. Contribution of Working Groups I, II and III to the Fifth Assessment Report of the Intergovernmental Panel on Climate Change, In, Geneva, Switzerland, 151, 2014.

Kaiser, K., Canedo-Oropeza, M., McMachon, R., and Amon, R. M. W.: Origins and transformations of dissolved organic matter in large Arctic rivers, Scientific Reports, 7, 1-11,

© Author(s) 2022. CC BY 4.0 License.


10.1038/s41598-017-12729-1, 2017.

Karlsson, J., Serikova, S., Vorobyev, S. N., Rocher-Ros, G., Denfeld, B. A., and Pokrovsky, O. S.: Carbon emission from Western Siberian inland waters, Nature Communications, 12, 1-8, 10.1038/S41467-021-21054-1, 2021.

Kling, G. W., Kipphut, G. W., and Miller, M. C.: The flux of CO_2 and CH_4 from lakes and rivers in arctic Alaska, Hydrobiologia, 240, 23-26, 10.1007/BF00013449, 1992.

Kwon, M. J., Beulig, F., Ilie, I., Wildner, M., Küsel, K., Merbold, L., Mahecha, M. D., Zimov, N., Zimov, S., Heimann, M., Schuur, E. A., Kostka, J. E., Kolle, O., Hilke, I., and Göckede, M.: Plants, microorganisms, and soil temperatures contribute to a decrease in methane fluxes on a drained Arctic floodplain, Global Change Biology, 23, 2396-2412, 10.1111/gcb.13558, 2017.

Lammers, R. B., Shiklomanov, A. I., Vörösmarty, C. J., Fekete, B. M., and Peterson, B. J.: Assessment of contemporary Arctic river runoff based on observational discharge records, Journal of Geophysical Research, 106, 3321-3334, 10.1029/2000JD900444, 2001.

Mann, P. J., Strauss, J., Palmtag, J., Dowdy, K., Ogneva, O., Fuchs, M., Bedington, M., Torres, R., Polimene, L., Overduin, P. P., Mollenhauer, G., Grosse, G., Rachold, V., Sobczak, W. V., Spencer, R. G. M., and Juhls, B.: Degrading permafrost river catchments and their impact on Arctic Ocean nearshore processes, Ambio, 51, 439-455, 10.1007/s13280-021-01666-z, 2022.

Mansour, I., Heppell, C. M., Ryo, M., and Rilling, M. C.: Application of the microbial community coalescence concept to riverine networks, Biological Reviews of the Cambridge Philosophical Society, 93, 1832-1845, 10.1111/brv.12422, 2018.

Mincer, T. J. and Aicher, A. C.: Methanol production by a broad phylogenetic array of marine phytoplankton, PLoS ONE, 11, e0150820, 10.1371/journal.pone.0150820, 2016.

Olefeldt, D., Turetsky, M. R., Crill, P. M., and McGuire, A. D.: Environmental and physical controls on northern terrestrial methane emissions across permafrost zones, Global Change Biology, 19, 589-603, 10.1111/gcb.12071, 2013.

Olid, C., Zannella, A., and Lau, D. C. P.: The role of methane transport from the active layer in sustaining methane emissions and food chains in subarctic ponds, Journal of Geophysical Research: Biogeosciences, 126, e2020JG005810, 10.1029/2020JG005810, 2021.

Raymond, P. A., Zappa, C. J., Butman, D., Bott, T. L., Potter, J. D., Mulholland, P., Laursen, E., McDowell, W. H., and Newbold, D.: Scaling the gas transfer velocity and hydraulic geometry in streams and small rivers, Limnology and Oceanography: fluids and environments, 2, 41-53, 10.1215/21573689-1597669, 2012.

Rosentreter, J. A., Borges, A. V., Deemer, B. R., Holgerson, M. A., Liu, S., Song, C., Melack, J. M., Raymond, P. A., Duarte, C. M., Allen, G. H., Olefeldt, D., Poulter, B., Battin, T. I., and Eyre, D.: Half of global methane emissions come from highly variable aquatic ecosystem sources, Nature Geoscience, 14, 225-230, 10.1038/s41561-021-00715-2, 2021.

Saunois, M., Stavert, A. R., Bousquet, P., Canadell, J. G., and et al.: The global methane budget 2000-2017, Earth System Scientific Data, 12, 1561-1623, 10.5194/essd-12-1561-2020, 2020.

https://doi.org/10.5194/bg-2022-135
Preprint. Discussion started: 29 June 2022
© Author(s) 2022. CC BY 4.0 License.

Schuur, E. A., McGuire, D., Schädel, C., Grosse, G., Harden, J. W., Hayes, D. J., Hugelius, G., Koven, C. D., Kuhry, P., Lawrence, D. M., Natali, S. M., Olefeldt, D., Romanovsky, V. E., Schaefer, K., Turetsky, M. R., Treat, C. C., and Vonk, J. E.: Climate change and the permafrost carbon feedback, Nature, 520, 171-179, 10.1038/nature14338, 2015.

Shakhova, N. and Semiletov, I. P.: Methane release and coastal environment in the East Siberian Arctic shelf, Journal of Marine Systems, 66, 227-243, 10.1016/j.jmarsys.2006.06.006, 2007.

Shakirov, R. B., Mau, S., Mishukova, G. I., Obzhirov, A. I., Shakirova, M. V., and Mishukova, O. V.: The features of methane fluxes in the western and eastern Arctic: a review. Part I, Geosystems of Transition Zones, 4, 004-025, 10.30730/2541-8912.2020.4.1.004-025, 2020.

Snyder, L., Potter, J. D., and McDowell, W. H.: An evaluation of nitrate, fDOM, and turbidity sensors in New Hampshire Streams, Water Resources Research, 54, 2466-2479, 10.1002/2017WR020678, 2018.

Stanley, E. H., Casson, N. J., Christel, S. T., Crawford, J. T., Loken, L. C., and Oliver, S. K.: The ecology of methane in streams and rivers: patterns, controls, and global significance, Ecological Monographs, 86, 146-171, 10.1890/15-1027, 2016.

Striegl, R. G., Dornblaser, M. M., McDonald, C. P., Rover, J. R., and Stets, E. G.: Carbon dioxide and methane emissions from the Yukon River System, Global Biogeochemical Cycles, 26, GB0E05, 10.1029/2012GB004306, 2012.

Turetsky, M. R., Abbott, B. W., Jones, M. C., Walter Anthony, K., Olefeldt, D., Schuur, E. A., Grosse, G., Kuhry, P., Hugelius, G., Koven, C., Lawrence, D. M., Gibson, C., Sannel, A. B., and McGuire, D.: Carbon release through abrupt permafrost thaw, Nature Geoscience, 13, 138-143, 10.1038/s41561-019-0526-0, 2020.

Vigneron, A., Cruaud, P., Bhiry, N., Lovejoy, C., and Vincent, W. F.: Microbial community structure and methane cycling potential along a thermokarst pond-peatland continuum, Microorganisms, 7, 10.3390/microorganisms7110486, 2019.

Vorobyev, S. N., Karlsson, J., Kolesnichenko, Y. Y., and Koretz, M.: Fluvial carbon dioxide emission from the Lena River basin during spring flood, Biogeosciences Discussions, doi: 10.5194/bg-2021-109, 2021. 10.5194/bg-2021-109, 2021.

Wanninkhof, R.: Relationship between gas exchange and wind speed over the ocean, Journal of Geophysical Research, 97, 7373-7381, 10.1029/92JC00188, 1992.

Wanninkhof, R.: Relationship between wind speed and gas exchange over the ocean revisited, Limnology and Oceanography: Methods, 12, 351-362, 10.4319/lom.2014.12.351, 2014.

Watras, C. J., Hanson, P. C., Stacy, T. L., Morrison, K. M., Mather, J., Hu, Y.-H., and Milewski, P.: A temperature compensation method for CDOM fluorescence sensors in freshwater, Limnology and Oceanography Methods, 9, 296-301, 10.4319/lom.2011.9.296, 2011.

Weiss, R. F.: The solubility of nitrogen, oxygen and argon in water and sea water, Deep Sea Research, 17, 721-735, 10.1016/0011-7471(70)90037-9, 1970.

https://doi.org/10.5194/bg-2022-135
Preprint. Discussion started: 29 June 2022
© Author(s) 2022. CC BY 4.0 License.


Wiesenburg, D. A. and Guinasso, J. N. L.: Equilibrium solubilities of methane, carbon monixide, and hydrogen in water and sea water, Journal of Chemical and Engineering Data, 24, 356-360, 10.1021/cr60306a003, 1979.

Wik, M., Varner, R. K., Walter Anthony, K., MacIntyre, S., and Bastviken, D.: Climate-sensitive northern lakes and ponds are critical components of methane release, Nature Geoscience, 99-106, 10.1038/NGEO2578, 2016.

Xin, J., Zhang, Y., Zhang, S., Xia, C., and Li, S.: Methanol production from CO_2 by resting cells of the methanotrophic bacterium *Methylosinus trichosporium* IMV 3011, Journal of Basic Microbiology, 47, 426-435, 10.1002/jobm.200710313, 2007.

Zolkos, S., Tank, S. E., Striegl, R., and Kokelj, S. V.: Thermokarst effects on carbon dioxide and methane fluxes in streams on the Peel Plateau (NWT, Canada), Journal of Geophysical Research: Biogeosciences, 124, 1781-1798, 10.1029/2019JG005038, 2019.

https://doi.org/10.5194/bg-2022-135
Preprint. Discussion started: 29 June 2022
© Author(s) 2022. CC BY 4.0 License.

Figures

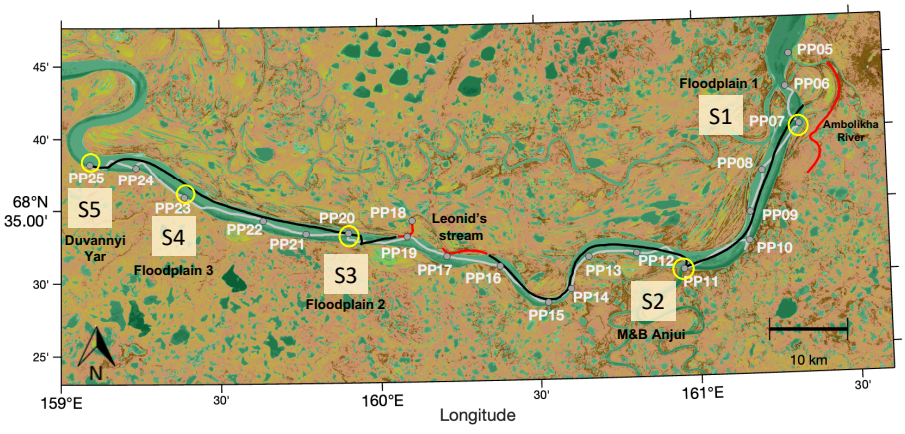

930 **Figure 1 –** Navigated transects in the Kolyma River: upstream (UP) (grey line, sampled from 15 June 2019 at 12:30 h to 16 June 2019 at 16:59 h) and downstream (DOWN) (black line, navigated on 16-17 June 2019). Gaps in the continuous UP and DOWN transects are data not considered for the analysis because they involved navigation outside the main river channel (i.e., transects at Leonid's stream and the Ambolikha River indicated in red). Discrete samples
935 were collected in 21 sampling stations (PP05-PP25) during the UP transect (grey markers). Key sites (and stations): S1 (PP07), S2 (PP11), S3 (PP20), S4 (PP23), and S5 (PP25) are circled in yellow. This map was created using MATLAB® with data from a composite image for June, July and August from 205-2018 using Sentinel-2 NDVI maps (https://developers.google.com/earth-engine/datasets/catalog/sentinel).
940

945

950

955

https://doi.org/10.5194/bg-2022-135
Preprint. Discussion started: 29 June 2022
© Author(s) 2022. CC BY 4.0 License.

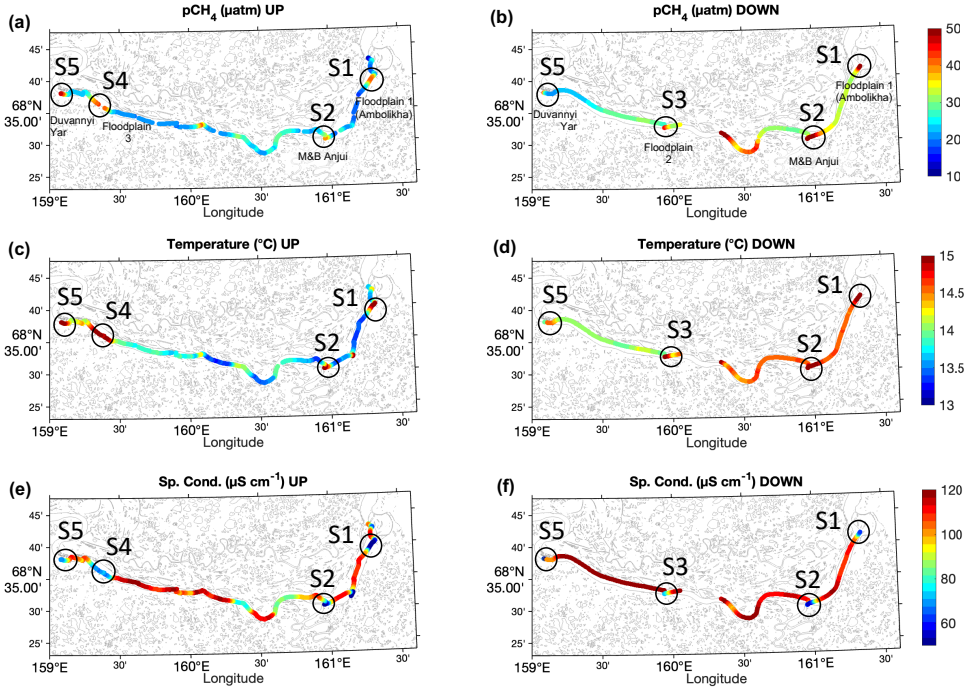

Figure 2 – Spatial distribution of water properties measured along transects UP (left) and DOWN (right) at the main stem of the Kolyma River for pCH_4 (a and b), T (c and d), and κ (e and f). The location of key sites S1 to S5 are indicated. The values corresponding to Ambolikha River and Leonid's stream are not shown.

https://doi.org/10.5194/bg-2022-135
Preprint. Discussion started: 29 June 2022
© Author(s) 2022. CC BY 4.0 License.

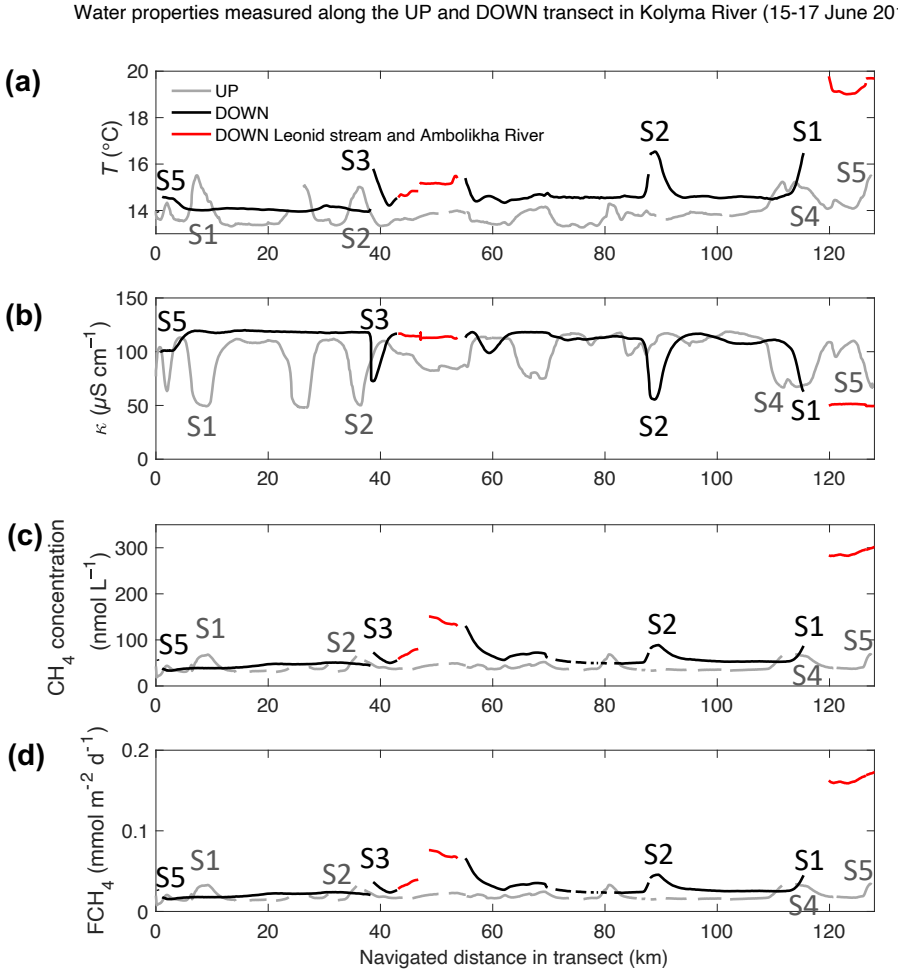

1010 **Figure 3** – Water properties measured in transects UP (grey) and DOWN (black): a) water temperature, *T*; b) water-specific conductivity, κ; c) CH_4 concentration, C_w, and d) flux density of CH_4, FCH_4, all shown as a function of the navigated distance (km) along each transect. The location corresponding to the key sites S1 to S5 are indicated and color-coded in each signal (light grey – UP transect and black – DOWN transect). The Ambolikha River and
1015 Leonid's stream are shown in red. Gaps in the data indicate erroneous or not measured data in the transect.

1020

https://doi.org/10.5194/bg-2022-135
Preprint. Discussion started: 29 June 2022
© Author(s) 2022. CC BY 4.0 License.

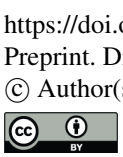

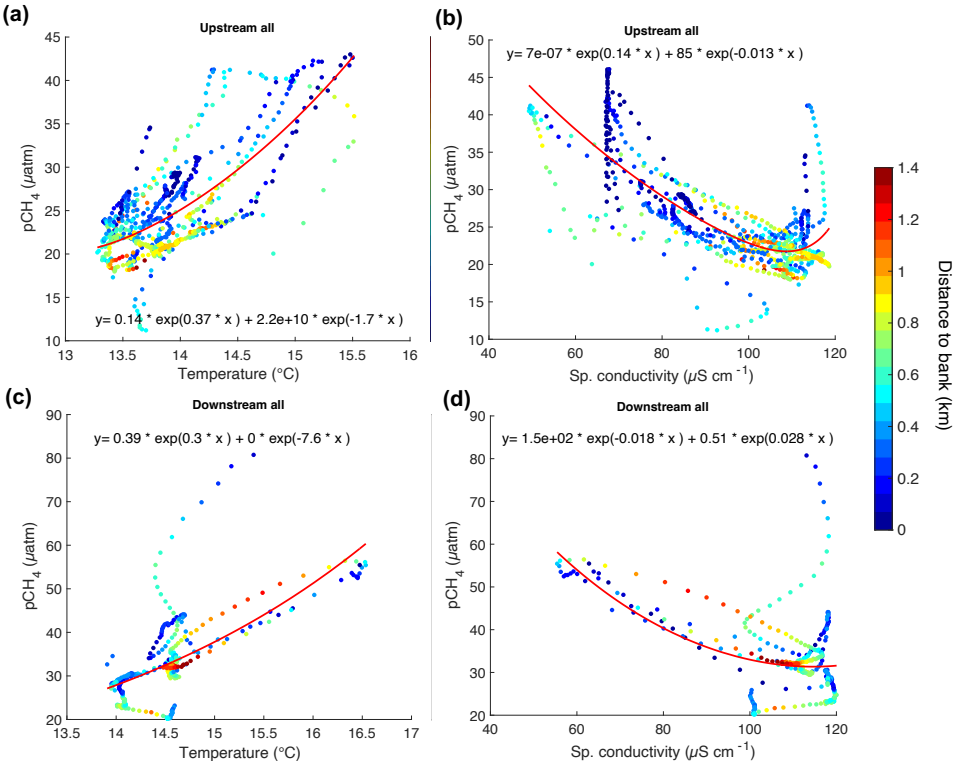

Figure 4 – Correlation graphs for UP (a and b) and DOWN (c and d) transects between T, κ and pCH_4 as a function of the distance to bank (z in km) indicated in the color scale.

https://doi.org/10.5194/bg-2022-135
Preprint. Discussion started: 29 June 2022
© Author(s) 2022. CC BY 4.0 License.

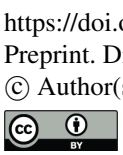

1055

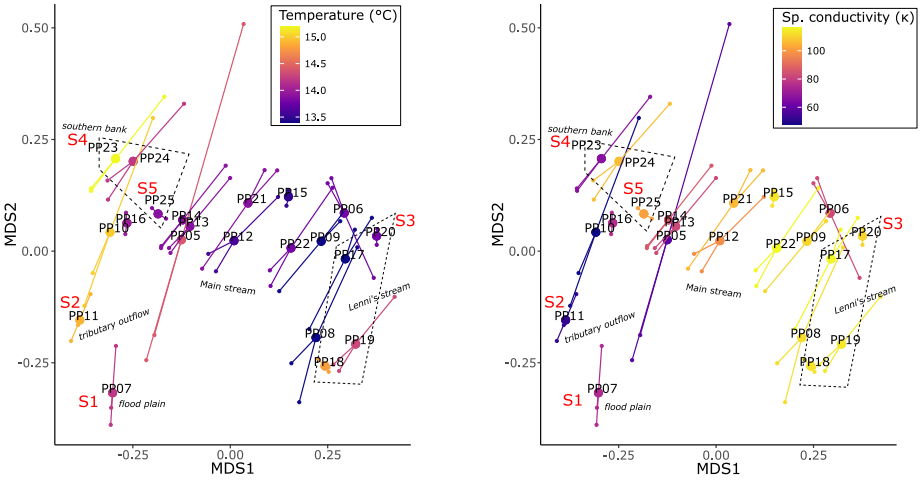

1060 **Figure 5** – Riverine microbial community composition linked to temperature (left) and specific conductivity (right). Both plots represent the same underlying community data, with dissimilarities determined by the Bray-Curtis metric and visualized with non-metric multidimensional scaling plots.

1065

1070

1075

1080

1085

https://doi.org/10.5194/bg-2022-135
Preprint. Discussion started: 29 June 2022
© Author(s) 2022. CC BY 4.0 License.

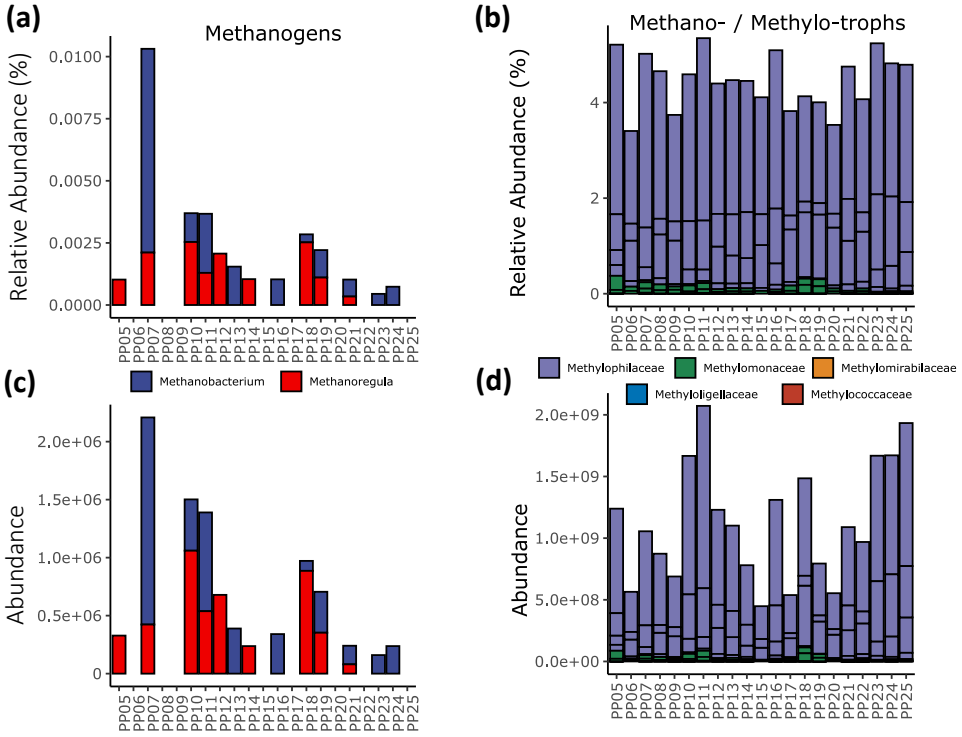

1090 **Figure 6** – Relative (top) and pseudo-absolute (bottom) abundances of putatively methanogenic archaeal genera (left) and methylotrophic bacterial families (right). An expanded version that includes only the methanotrophs is available in the supplemental information.

1095

1100

1105

1110

https://doi.org/10.5194/bg-2022-135
Preprint. Discussion started: 29 June 2022
© Author(s) 2022. CC BY 4.0 License.

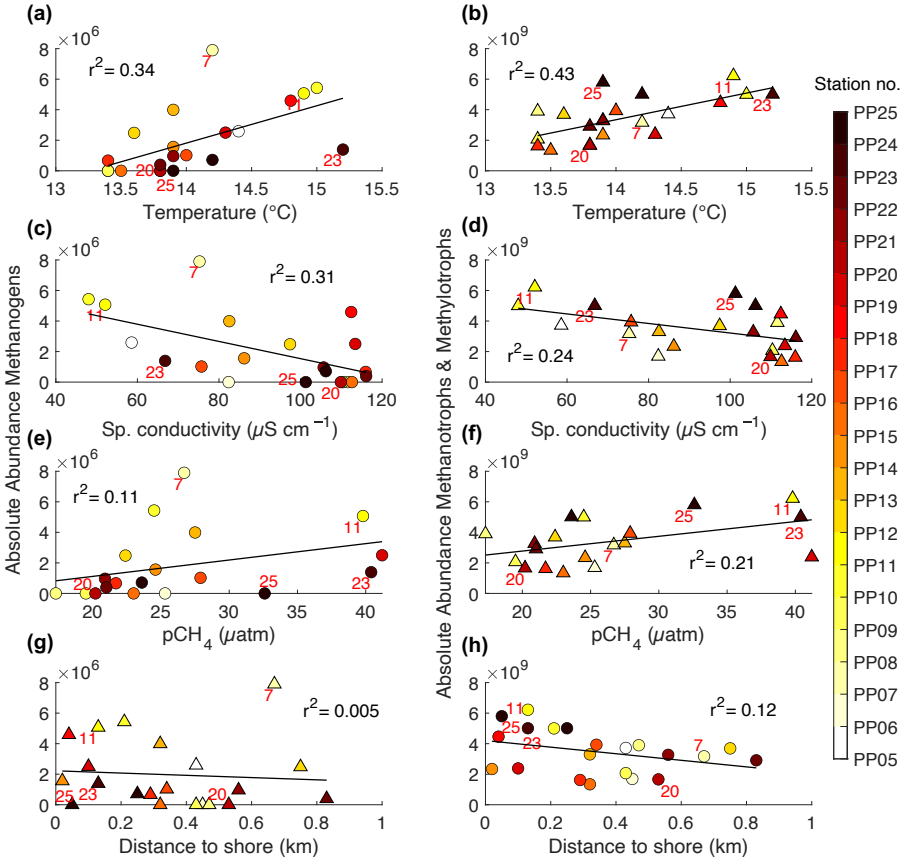

Figure 7 – Linear correlations between the total absolute abundances of archaeal microbial communities (left, methanogens and right, methanotrophs) and the 1-min averages of water properties measured at the 21 sampling stations along the DOWN transect in Kolyma River. Red numbers in some of the markers indicate the station number corresponding to the key sites S1 to S5.

https://doi.org/10.5194/bg-2022-135
Preprint. Discussion started: 29 June 2022
© Author(s) 2022. CC BY 4.0 License.

Biogeosciences
Discussions
Open Access
EGU

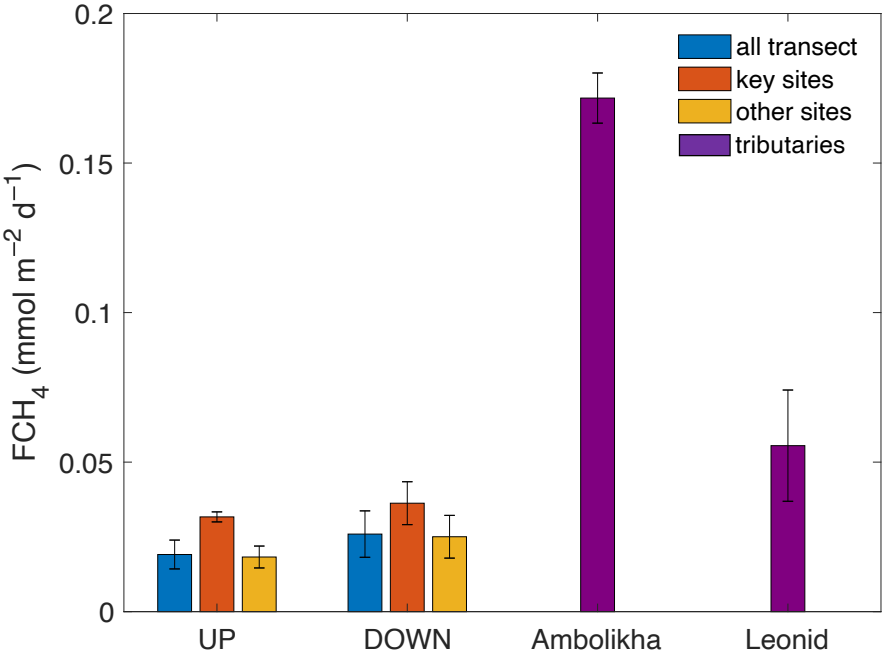

1135

Figure 8 – Average flux density of CH_4 (FCH_4) calculated for the entire UP and DOWN transects, and for the key sites and other sites. FCH_4 for the tributaries Ambolikha River and Leonid's stream are also shown. Error bars denote the standard deviation of the mean.

1140

https://doi.org/10.5194/bg-2022-135
Preprint. Discussion started: 29 June 2022
© Author(s) 2022. CC BY 4.0 License.

Table 1 – Average ± 1 std. deviation (minimum and maximum values below it) of pCH_4, the concentration of CH_4 (C_w), T and κ measured along the UP and DOWN transects in key sites (S1 – S5) and in the other sites of each transect. Measurements done in a tributary (Ambolikha River) and a stream (Leonid's stream) as part of the measurements during the DOWN transect are also shown.

Location	**pCH_4 (µatm)**	**C_w (nmol L^{-1})**	**T (°C)**	**κ (µS cm^{-1})**
Both transects	28.3±8.5 (11.2 – 80.7)	45.9±12.9 (18.9 – 130.2)	14.1±0.6	96.8±21.5
UP transect	25.8±6.7 (11.2 – 46.1)	41.5±9.2 (18.9 – 69.2)	13.9±0.6	92.2±22.2
UP key sites	39.4±4.3	65.0±3.0	14.9±0.3	65.1±6.9
UP other sites	23.8±4.3	39.9±7.0	13.9±0.5	95.8±20.9
DOWN transect	33.2±9.4 (20.2 – 80.7)	54.3±14.7 (33.3 – 130.2)	14.5±0.5	108.3±14.5
DOWN key sites	42.8±9.2	72.4±12.4	15.7±0.8	76.0±16.0
DOWN other sites	31.8±8.5	52.7±13.7	14.4±0.3	112.4±7.3
Ambolikha River (DOWN)	206.8±9.8 (191.7 – 222.9)	300.7±12.1 (282.2 – 320.7)	19.6±0.3	49.9±0.9
Leonid's stream (DOWN)	66.8±22.0 (37.0 – 92.9)	111.1±35.7 (60.8 – 150.7)	15.1±0.3	113.9±1.6